Journal of Fluids and Structures (1994) **8**, 621–625

AN EXPERIMENTAL INVESTIGATION OF STREAMWISE VORTICES IN THE WAKE OF A BLUFF BODY

J. WU AND J. SHERIDAN
Monash University, Department of Mechanical Engineering
Clayton, Victoria 3168, Australia

AND

J. SORIA AND M. C. WELSH
Commonwealth Scientific and Industrial Research Organisation
Division of Building, Construction and Engineering
Highett, Victoria 3190, Australia

(Received 23 July 1993 and in revised form 2 December 1993)

Three-dimensional near-field wake structures behind a circular cylinder were investigated at Reynolds numbers ranging from 50 to 1800 based on cylinder diameter. The main feature of the three-dimensional structure of the wake behind the cylinder is the formation of streamwise vortices superimposed on the Strouhal vortex street. Flow visualization experiments were conducted to illustrate the relationship between the streamwise vortices and the Strouhal vortices. The formation of the streamwise vortices in the wake is discussed and it is emphasized that the stretching effect in the saddle region formed by the spanwise vortices plays a major role in the development of the streamwise vortices. Spanwise wavelengths of the streamwise vortices were measured using flow visualization and a digital imaging method. Spanwise perturbations were introduced to study the wavelength selectivity of the streamwise vortices.

1. INTRODUCTION

SINCE THE FIRST DISCOVERY of the von Kármán vortex street early this century, vortex shedding from a circular cylinder has been the subject of numerous investigations. This is due to its fundamental importance in research on the physics of fluids and its close link to many practical industrial applications, such as the heat transfer process in heat exchangers, wind loading on buildings, and many others.

Grant (1958) used hot-wire anemometry and cross-correlation techniques to study the wake behind a circular cylinder in a two-dimensional cross-flow, and he was perhaps the first to realize that Kármán vortices develop a three-dimensional vortical structure composed of counter-rotating streamwise vortices. Gerrard (1978) used a dye flow visualization technique to investigate flow behind a circular cylinder at low Reynolds number range. He observed "fingers" forming along the span of the cylinder when $Re > 140$. The "fingers" shown in his side-view photographs were distorted spanwise vortices made visible by dye. The findings were consistent with the earlier discovery of Hama (1957) who studied the three-dimensionality of the wake of a cylinder and found that a "transverse waviness" began to appear when Re was greater than 150. It is not difficult to conclude from their photographs that the "transverse waviness" and "fingers" are identical phenomena. They are indicative of the formation of streamwise vortices in the wake. Direct visual evidence of the existence of the

0889–9746/94/060621 + 15 $08.00

streamwise vortices in the near wake behind a cylinder have been provided in recent years by the flow visualization results of Wei & Smith (1986), Williamson (1988) and Welsh *et al.* (1992). Bays-Muchmore & Ahmed (1993) showed, using flow visualizations, that the streamwise vortices in the wake of a circular cylinder exist in the Reynolds number range from 330 to 21,000. They confirmed the findings of Williamson (1988) that the spanwise spacing of the streamwise vortices is approximately one cylinder diameter.

It is generally agreed that the phenomenon is caused by the internal instability of the base flow; the base flow is the vortex street in the case of wakes and spanwise rollers in the case of mixing layers. However, the mechanism whereby streamwise vortices are formed is still an open question. Pierrehumbert & Widnall (1982) studied an array of Stuart vortices using linear stability analysis and showed the existence of what they called the "translative instability" of the vortex cores. This instability mechanism has been used by many authors [e.g., Bernal & Roshko (1986), Nygaard & Glezer (1991)] to explain the origin of streamwise vortices in plane mixing layers.

Wei & Smith (1986) suggested that the streamwise vortices in the wake of a cylinder are the result of three-dimensional distortions of the Kelvin–Helmholtz (KH) vortices in the separated shear layer from the cylinder.

Lin & Corcos (1984) found that strained vortex sheets are fundamentally unstable. The stretching effect is the main driving force in the amplification of the streamwise vortices. This has been further illustrated by Ashurst & Meiburg (1988) and Lasheras & Meiburg (1990) using vortex simulation. They demonstrated the important roles played by the spanwise vortices in the stretching and reorientation of the vorticity. The largest stretching of vorticity occurs in the saddle point region.

Coutanceau & Defaye (1991) reviewed flow visualization investigations by Gerrard (1978) and Williamson (1988), and suggested that the streamwise vortices are Taylor vortices, as set up in the classic case of two coaxial rotating cylinders. Hussain (1984) suggested that the high turbulence production near the saddle point is primarily due to the ribs (streamwise vortices) undergoing stretching. He speculated that the formation of these ribs might involve a Taylor–Görtler type instability.

Yokoi & Kamemoto (1992) investigated the three-dimensional flow behind a circular cylinder using flow visualization techniques. They observed that the distances between neighbouring streaklines became narrower or wider downstream of the separation line, indicating the formation of streamwise vortices. They suggested that a three-dimensional boundary layer separation sets up the streamwise vortices.

In the present experimental investigation, carried out in a water tunnel, the development of streamwise vortices in the near wake region of a circular cylinder has been observed. Typical flow patterns showing the streamwise vortex structures are shown in Figures 1(a,b) and 2(a,b). These photographs were obtained using flow visualization. The vortices are found located in braids joining the spanwise Strouhal vortices. The vortex tubes are under continuous stretching by the Strouhal vortices, contributing to the increase in the streamwise vorticity. It has been postulated (Ferre *et al.* 1990) that this increase in streamwise vorticity contributes to the generation of fine-scale turbulence by transferring large-scale kinetic energy to small-scale turbulent kinetic energy.

Streakline visualization in unsteady flow can be misleading as has been noted by many authors, e.g. Hama (1962) and more recently Coutanceau & Defaye (1991). The flow patterns in the visualization show the integrated effect of the particle paths. This can result in the erroneous conclusion that rolling-up tracer patterns represent vortex structures. The problem can be avoided (or minimized) by releasing the tracers as

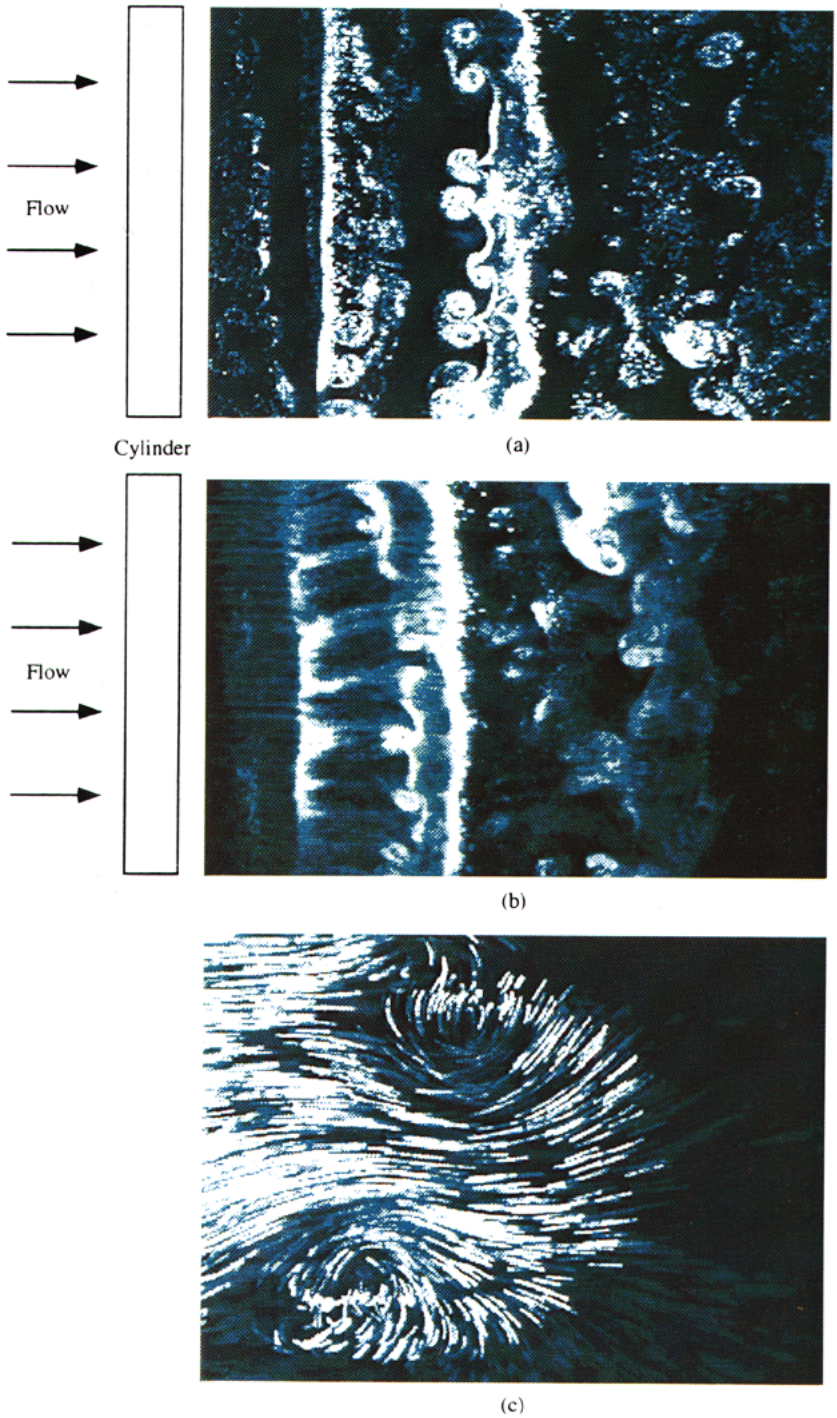

Figure 1. Streamwise vortices embedded in the Strouhal vortices: the pictures were recorded by camera 'B' illuminated with laser sheet 'B' (refer to the experimental set-up diagram, Figure 3); $D = 12{\cdot}0$ mm, Re = 1000, flow from left to right.

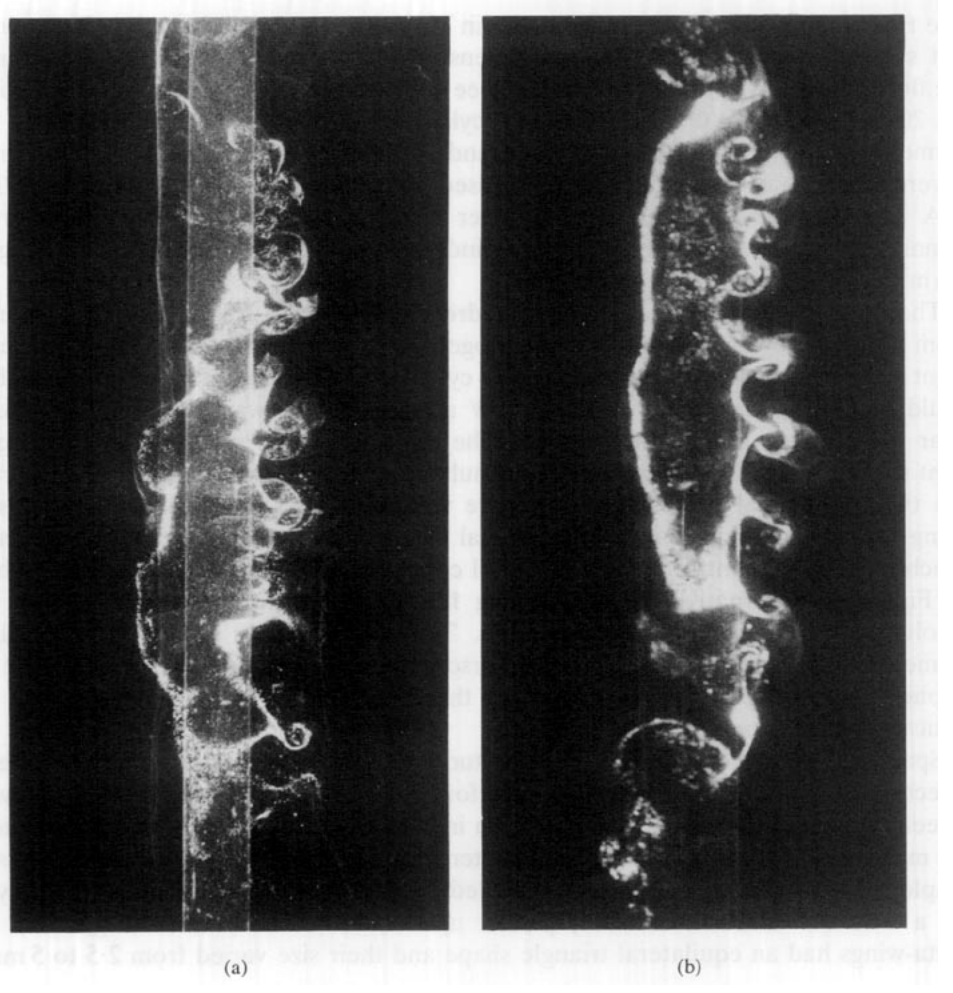

Figure 2. Streamwise vortices embedded in the Strouhal vortices, looking upstream at a plane $4D$ behind the cylinder; D = 12·0 mm, Re = 1000.

close as possible to the region of vorticity generation. In the current study, attention was focused in the near wake region immediately behind the cylinder close to where the tracers were released, thus reducing the above-mentioned error. Nevertheless, caution is needed in interpreting visualized patterns in the far wake region, where bias can be large.

In this paper we present experimental results, mainly in the form of flow visualizations, aimed at understanding the physical structure of the streamwise vortices. Spanwise wavelength measurements of the streamwise structures in natural as well as forced shedding are also presented.

2. EXPERIMENTAL FACILITIES AND PROCEDURES

A return-circuit type water tunnel was used for experiments. Water was pumped into a settling chamber containing filter material and a honeycomb and then passed through a 4:1 contraction before entering the working section, which is 770 mm long with a 244 × 244 mm cross-section. The walls of the test section are made of transparent acrylic material. The maximum mean flow velocity in the working section is 400 mm/s.

The freestream velocity was uniform within 1% outside the wall boundary layers in the test section. Longitudinal turbulence intensity was typically 0·15%. The spectrum of the fluctuating longitudinal velocity was free of sharp peaks and decreased in amplitude by 20 dB/Hz above 0·08 Hz. Circular cylinders made of polished plexiglass with diameters ranging from 3·3 to 12·7 mm and 244 mm long were used. The experiment covered a range of Reynolds numbers, based on cylinder diameter, from 50 to 1800.

A TSI hot-film sensor and anemometer were used to detect the phase reference signal of the vortex shedding from the cylinder. The hot-film sensor was 1 mm long and 4 μm in diameter.

The flow visualization method used hydrogen bubbles as tracer particles, generated from a nichrome wire cathode. The hydrogen bubble wire was positioned 90° from the front stagnation point and 1 mm from the cylinder surface, so that the sheet of bubbles could be entrained into the wake. A 4 W argon-ion laser was used to illuminate the near wake region behind the cylinder. The laser beam was split into two orthogonal light sheets. Images could be recorded simultaneously with two digital CCD cameras in the two orthogonal planes. The exposure was controlled by pulsing the laser sheet using an acoustic-optical modulator. Digital image recording and laser illumination was synchronized and controlled by a personal computer; the experimental set-up is shown in Figure 3. Alternatively, time varying flow patterns were recorded with a high resolution CCD camera on video tape. The video images were digitized with a frame-grabber system operating on a personal computer. Digital image analysis was applied to the digital images to extract the flow features and to measure the flow structural dimensions.

Spanwise perturbations were used to study their effect on the spanwise wavelength selection of the streamwise vortices. Two forms of perturbations were used. One was a screen made of a thin wire array as shown in Figure 4. Cotton wires with a diameter of 0·5 mm and nichrome wires with a diameter of 0·06 mm were used. The other method employed an array of delta-wings installed at an attack angle of approximately 20° on a wire (0·1 mm in diameter) placed upstream of the cylinder (Figure 4). The delta-wings had an equilateral triangle shape and their size varied from 2·5 to 5 mm.

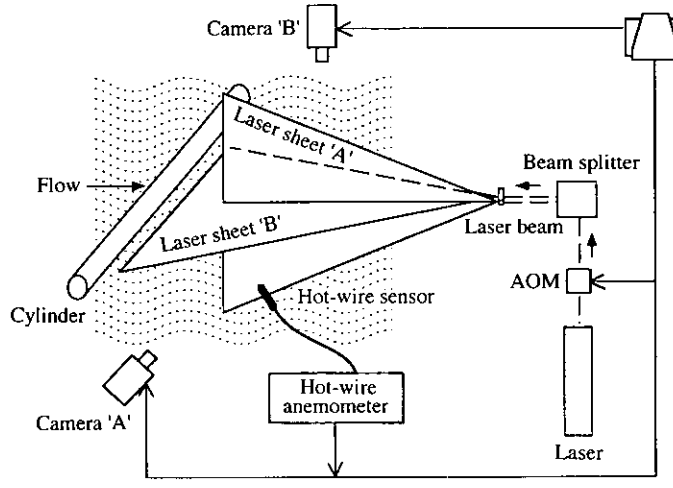

Figure 3. The experimental set-up: two orthogonal laser sheets illuminate the near wake region behind the cylinder; two digital CCD cameras are used to simultaneously record the flow patterns in the two image planes; the flow is visualized using hydrogen bubbles.

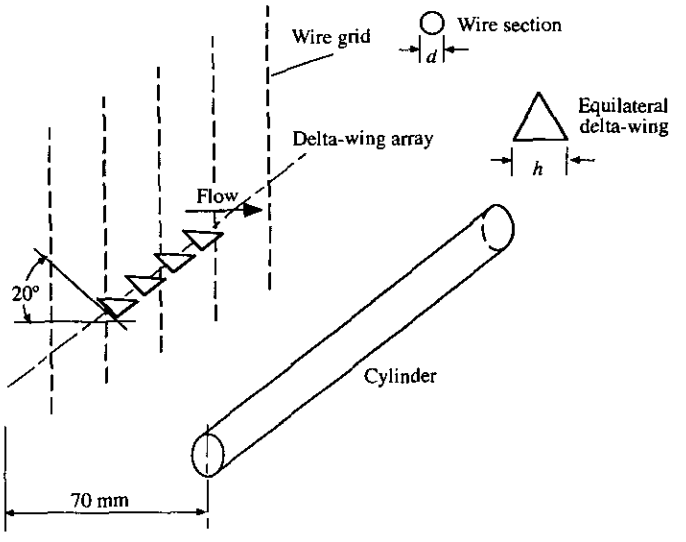

Figure 4. Spanwise perturbation arrangement: delta-wing and wire grid.

It is important to show that the observed phenomenon is "natural" and not caused by some imperfections in the experiments, such as disturbances due to tunnel vibration or residual turbulence from the upstream screen. Either of these might result in the observed structures. To overcome these factors in these experiments, circular cylinders of different diameters were tested under the same flow conditions. The spanwise wavelength of the structures was found to change as the diameter of the cylinder was varied. This helped to establish confidence that the observed flow structures were general features of the flow.

The wake of a bluff body can be influenced by end effects. One symptom of such an influence is the oblique vortex shedding mode discussed by Williamson (1989). He demonstrated that the end-effects can be minimized by arranging the end-plates at an inclined angle, inducing a parallel vortex-shedding mode. His method was used here with a pair of end-plates placed at an angle of 25° to the streamwise direction to ensure a parallel vortex shedding, thus minimizing end-effects. The streamwise vortices were found to exist even with parallel shedding of the Strouhal vortices, indicating that the existence of the streamwise vortices is not sensitive to the end-effects.

Typically each realization of the spanwise wavelength measurements from the digital image had a standard deviation of 15%, with 50 images normally used to obtain an average. This results in an uncertainty in the mean spanwise wavelength measurements of less than ±5% at a 95% confidence level.

3. EXPERIMENTAL RESULTS

3.1. Preview of the Flow Structures

Typical spanwise flow patterns showing the formation of streamwise counter-rotating vortices are presented in Figures 1(a,b,c) and 2(a,b). In Figure 1(a,b), the flow patterns in a plane parallel to the freestream velocity and to the axis of the cylinder were photographed at two typical Strouhal shedding phases. Figure 1(a) shows the

mushroom-type structures across the span of the cylinder developing behind the cylinder. At other phase times in the shedding cycle [Figure 1(b)], the mushroom-type structures are less clear, but the rib-like structures are evident.

Figure 1(c) is an enlarged photograph showing the characteristic mushroom shape that results when hydrogen bubbles are entrained into the streamwise vortices.

Figure 2(a,b) shows a cross-flow view looking upstream at the three-dimensional structures in a plane $4D$ downstream of the cylinder at Re = 1000 at two arbitrary time instants. The mushroom-type structures are on the right side and the vertical illuminated line is part of the Strouhal vortex.

3.2. Time-evolution of the Streamwise Vortices

A time sequence of still pictures (Figure 5) shows the three-dimensional vortex shedding process over more than one vortex-shedding cycle ($t = 0{\cdot}0 \sim 1{\cdot}3T$, where T is the period of vortex shedding). The images were recorded at the standard video rate (25 Hz). The time interval between consecutive frames is $0{\cdot}11T$; the Reynolds number is 440. The diameter of the cylinder was 9·4 mm, and it was located on the left side of the picture. Flow is from left to right. The plane of view coincides with the plane containing the axis of the cylinder. The pictures cover a spanwise area of approximately 12 diameters of the cylinder. The experimental set-up is schematically shown in Figure 3, with laser sheet 'B' active, and the video camera positioned at the place denoted camera 'B'.

The vertical structures shown in Figure 5 are the Strouhal vortices shed from the cylinder. The streamwise vortices can be found along the span of the vertical Strouhal vortex structures. At the phase $t = 0{\cdot}22 \sim 0{\cdot}44T$, the streamwise vortices are just being cut by the laser sheet across their sections, resulting in mushroom-type structures (indicated by white arrows). This is indicative of the counter-rotating nature of these structures. At other Strouhal shedding phases (e.g. $t = 0.88 \sim 1.10T$), the mushroom structures are not in focus. However, their relationship to the consecutive Strouhal vortices can be inferred from the rib-like structures (indicated by yellow arrows) joining neighbouring Strouhal vortices; the rib-like structures are seen when the counter-rotating streamwise vortex tubes are lying approximately in a plane parallel to the laser sheet. The mushroom-type structures become visible again at $t = 1{\cdot}21 \sim 1{\cdot}32T$, after one period of the vortex-shedding cycle, indicating that the streamwise vortices have the same frequency as the Strouhal vortices. The spanwise spacing of the streamwise vortices was approximately of the same order as the cylinder diameter, estimated from the photographs. More accurate measurement will be presented later in this paper.

3.3. Topology of the Streamwise Vortices

In order to examine the spatial relationship betwen the Strouhal vortices and the streamwise vortices, images in two orthogonal planes were acquired simultaneously using two CCD cameras (refer to Figure 3 for the experimental arrangement). The field of view began $0{\cdot}5D$ downstream of the cylinder, and covered an area of $(5{\cdot}5 \times 4{\cdot}4D)$ and $(5{\cdot}5 \times 5{\cdot}5D)$ for cameras 'A' and 'B' respectively.

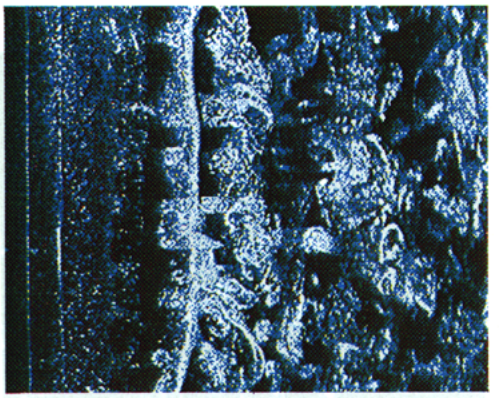

$t/T = 0{\cdot}11$

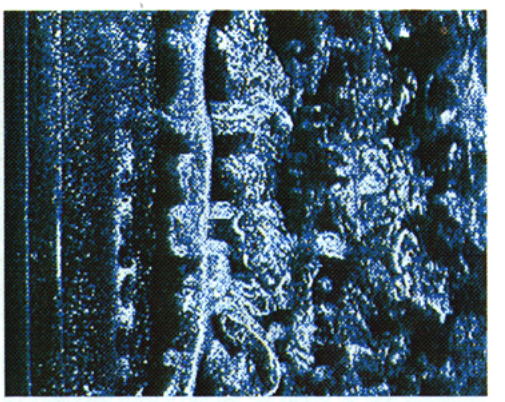

$t/T = 0{\cdot}22$

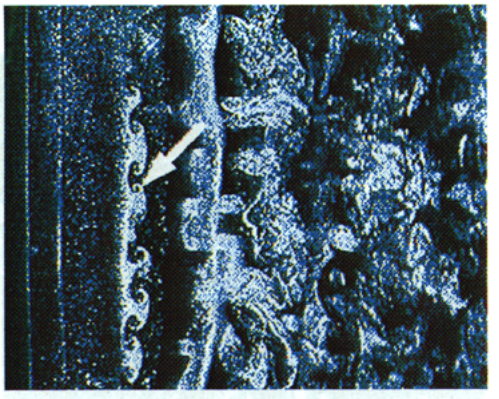

$t/T = 0{\cdot}33$

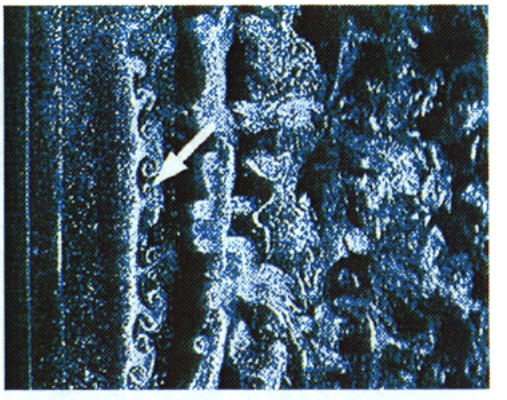

$t/T = 0{\cdot}44$

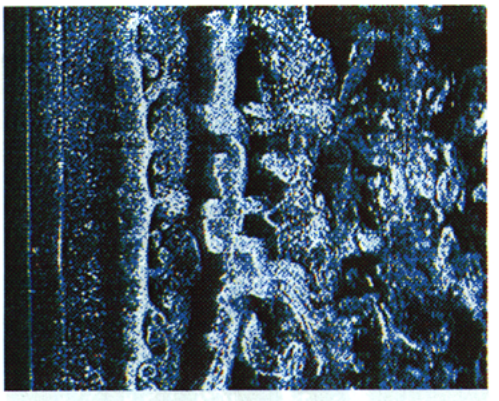

$t/T = 0{\cdot}55$

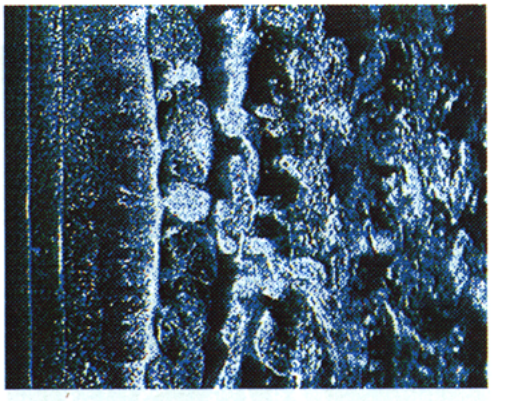

$t/T = 0{\cdot}66$

Figure 5. Time sequences showing three-dimensional vortex structures developing in the near wake of a circular cylinder: flow from left to right; the cylinder is at the left and its axis is in the plane of the picture; $D = 9{\cdot}4$ mm, Re = 440, t = time, T = Strouhal shedding period.

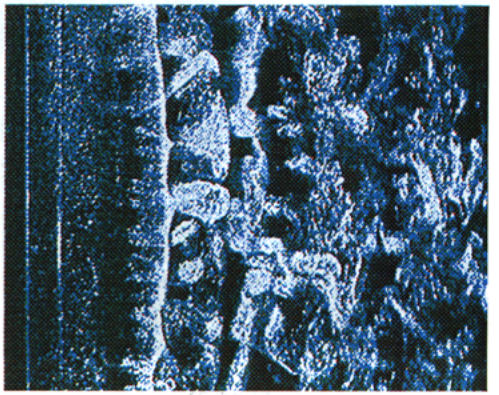

$t/T = 0{\cdot}77$

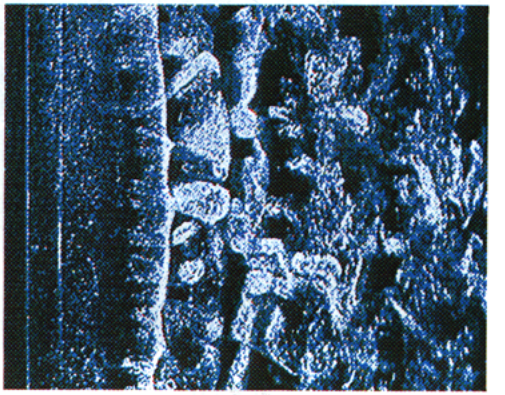

$t/T = 0{\cdot}88$

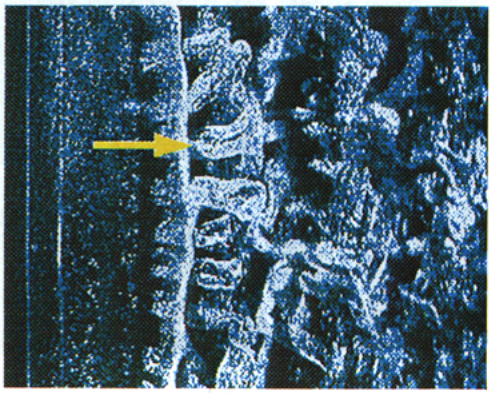

$t/T = 0{\cdot}99$

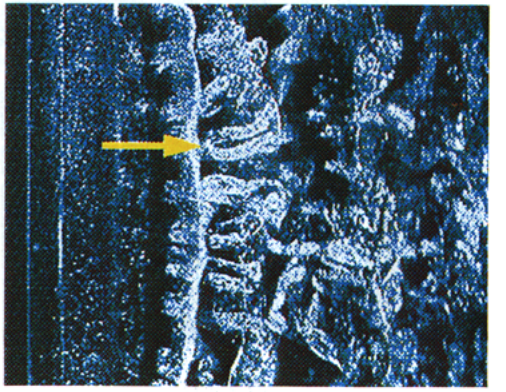

$t/T = 1{\cdot}10$

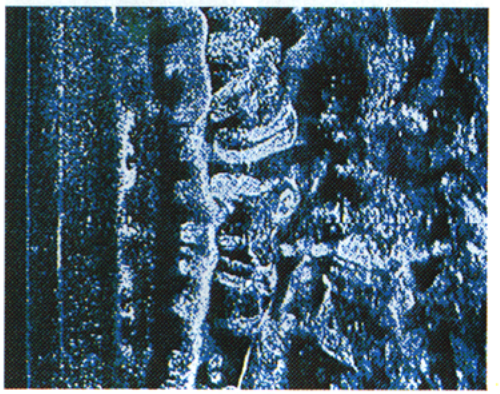

$t/T = 1{\cdot}21$

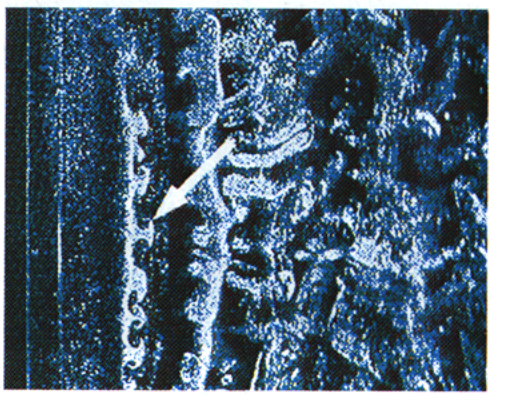

$t/T = 1{\cdot}32$

A typical result is shown in Figure 6(a,b). The arrows in the pictures indicate the location of the streamwise vortices. The white bars were due to the laser sheet in a plane normal to the current viewing plane. Figure 6(a) shows the spanwise Strouhal vortices; the arrow shows the position where braids containing counter-rotating streamwise vortices are cut by the laser sheet in the other plane. The flow pattern in the other plane recorded simultaneously is shown in Figure 6(b). Arrows in this plane show the mushroom-type structures being illuminated by laser sheet 'B' (Figure 3), supporting the idea that the streamwise vortices are residing in braids. Conceptual ideas interpreting these two pictures are shown in Figure 7(a,b).

In order to trace out the spatial orientation of the stramwise vortex tubes, a hot-film sensor was placed in the wake to trigger image acquisition, so that the images were recorded at the *same phase position* during the Strouhal vortex shedding cycle. Laser sheet 'B' (Figure 3) was then traversed laterally across the wake, and the distance from the centres of the mushroom-type structures to the cylinder was obtained from measurements of the digital images; the result is plotted in Figure 8. The two curves correspond to the two streamwise vortex tubes at a fixed Strouhal vortex-shedding phase position; the angles of tubes are not constant: the mean inclination angles are found to be approximately $55 \pm 5°$ to the streamwise direction and $-55 \pm 5°$.

3.4. Minimum Critical Reynolds Number Range

The critical Reynolds number, Re_{cr}, below which the streamwise vortices were not observed, was investigated using flow visualization. Observations focused on the near wake region extending up to $10D$ downstream of the cylinder. Three different cylinder diameters, i.e. 3·3, 6·4 and 9·4 mm, were used for the test. The results are graphed in Figure 9. The status of the streamwise vortices is divided into three levels: non-existent, intermittent and existent; digitally represented by -1, 0, $+1$, respectively. The intermittent status describes a situation where the vortices were found to exist intermittently. The streamwise vortices were not observed below the intermittent region of $Re \approx 150$–175, and were found to exist over the full cylinder span above this region. These results are in good agreement with the stability analysis of Noack *et al.* (1993) in which the onset of the three-dimensional instability was found to occur at $Re = 170$.

The use of end-plates did not affect Re_{cr}. This indicates that the onset of the stream wise vortices is not connected with Williamson's (1989) oblique vortex-shedding mode.

3.5. Spanwise Wavelength Measurement

The spanwise wavelength of the streamwise vortices is defined as the distance between the vortex pairs, as shown in Figure 10. Typical probability density distributions of the spanwise wavelength are shown in Figure 11. The figure shows that the spanwise wavelength, λ, depends on the cylinder diameter, D. i.e. λ increases with an increase in D.

Figure 12 shows the mean spanwise wavelength normalized by the diameter of cylinder as a function of Re. Five different cylinder diameters (3·3, 6·4, 9·4, 12·0 and 12·7 mm) were used. Each mean of λ was obtained by measuring approximately 50 randomly sampled digital images. The results show that the *mean* wavelength scales with the diameter of cylinder, and that the ratio λ/D varies slightly with Re for the parameter range used in these experiments. It should be noted, however, that the

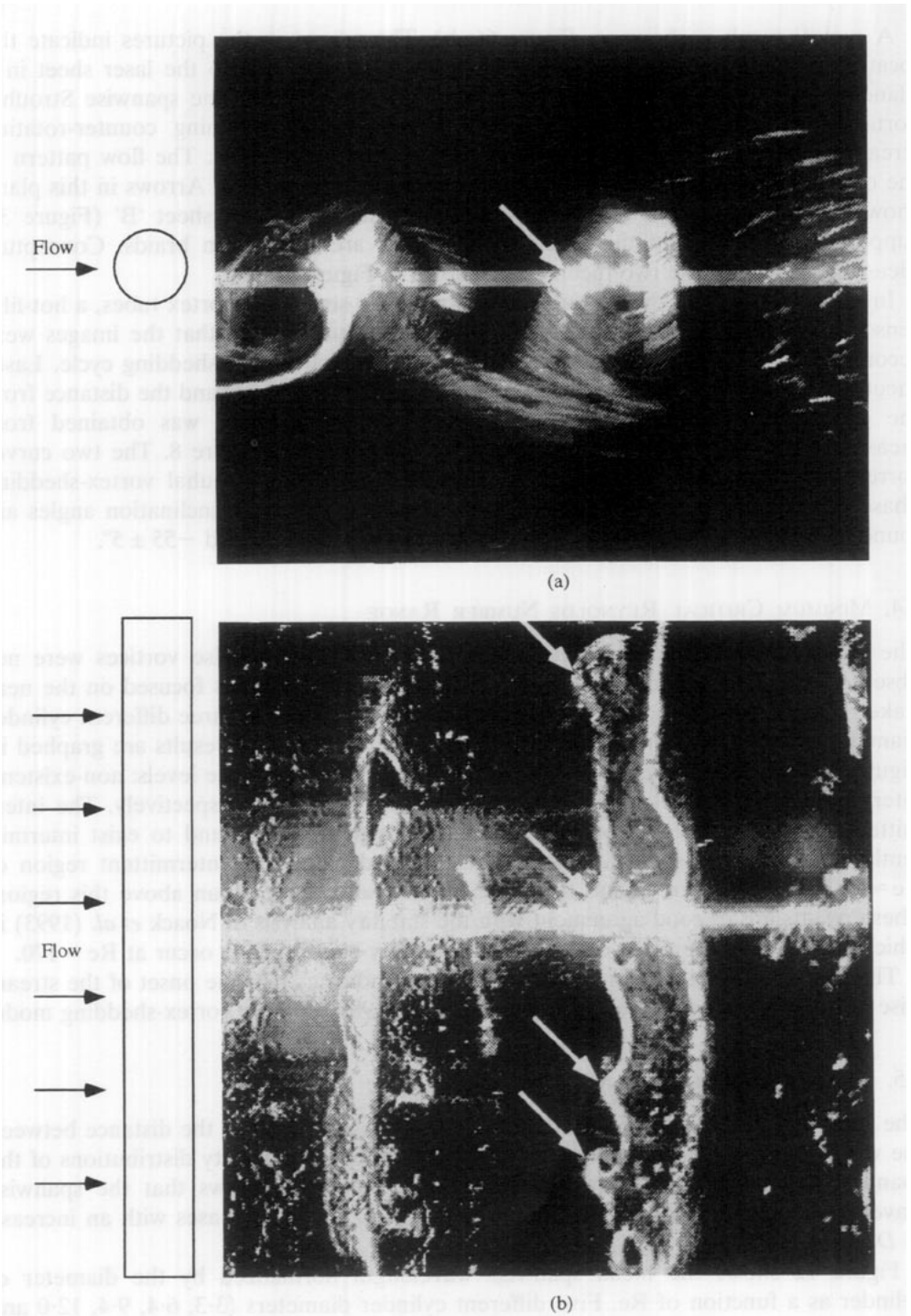

Figure 6. Two orthogonal plane views of the $3D$ wake (taken simultaneously): $D = 9{\cdot}4$ mm, $U = 0{\cdot}055$ m/s, Re = 440. (a) Strouhal vortices (taken by camera 'A'); (b) streamwise vortices (taken by camera 'B'). The arrows indicate locations of the streamwise vortices.

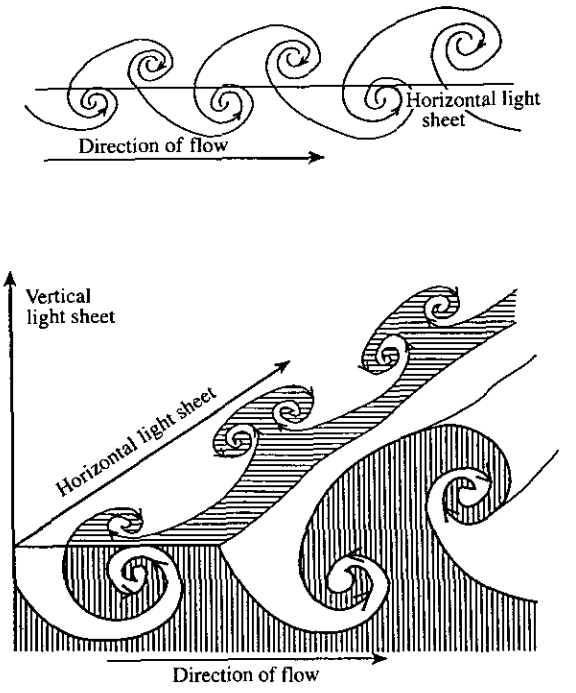

Figure 7. Conceptual diagram showing the flow structures being visualized: (a) Strouhal vortices (viewed by camera 'A'); (b) streamwise vortices embedded in the Strouhal vortex street (viewed by camera 'B'). Cross hatching indicates regions of rotational fluid.

individual realizations of λ have a high degree of uncertainty as is implied in the probability distribution (Figure 11) and that individual λ might deviate from scaling with D.

The value of λ/D varies from approximately 0·90–0·95 at Re $\approx$ 200 to 0·7–0·8 at higher Re (1000 ~ 1800). Data were not recorded between Re = 150 ~ 175 due to the intermittent existence of the streamwise vortices in this range. It is not entirely clear

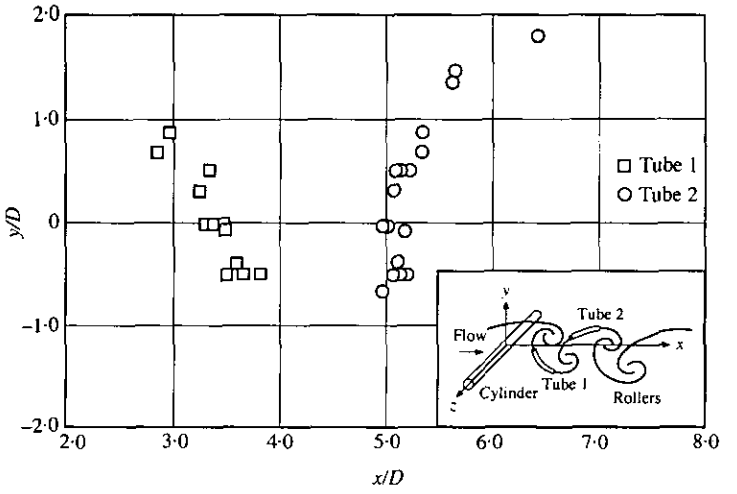

Figure 8. The mean location of the streamwise vortex tubes in the xy-plane was determined from xz-plane images. The images were acquired at a fixed phase in the Strouhal shedding cycle by traversing the laser sheet in the y-direction. D = 9·4 mm, U = 0·055 m/s, Re = 440.

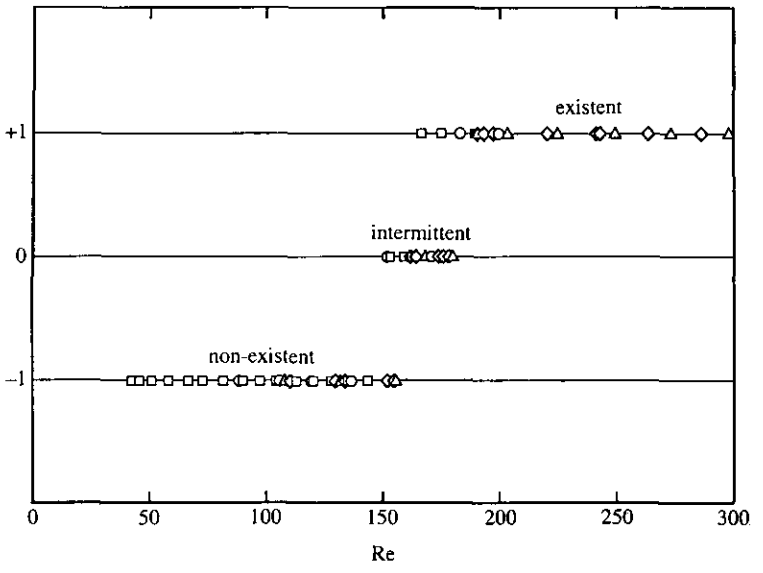

Figure 9. Onset of the streamwise vortices: effect of Reynolds number. The existence of the streamwise vortices: nonexistent, intermittent and existent, and represented by −1, 0, +1 respectively. ◇, $D = 9{\cdot}40$ mm; ○, $D = 6.45$ mm; □, $D = 3{\cdot}30$ mm; Δ, $D = 9{\cdot}4$ mm (angled end-plates).

whether this range is relevant to Williamson's (1988) "first stage", although we observed that within our intermittent range spacing between the streamwise vortices was much wider.

Noack *et al.* (1983) studied the onset of the three-dimensional instability using Floquet analysis. They found that the critical Floquet multiplier exhibits a sharp peak at a spanwise wavelength of $1{\cdot}8D$. This is higher than the values measured here but such a result would be expected if, as Williamson suggests, there is a *first stage* of longer spanwise wavelength between the onset at a Re = 170 and Re = 230. As noted earlier, the results presented here are at Reynolds numbers corresponding to the *second stage.* However, the finding of Noack *et al.* (1993) of a particularly sharp peak in the critical Floquet multiplier implies that at onset there is a dominant mode, implying it would be difficult to excite other wavelengths. This coincides with our results as discussed below.

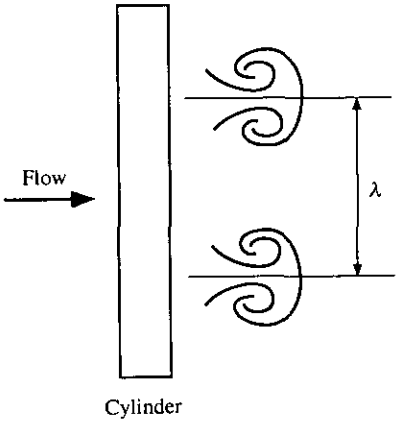

Figure 10. The definition of spanwise wavelength.

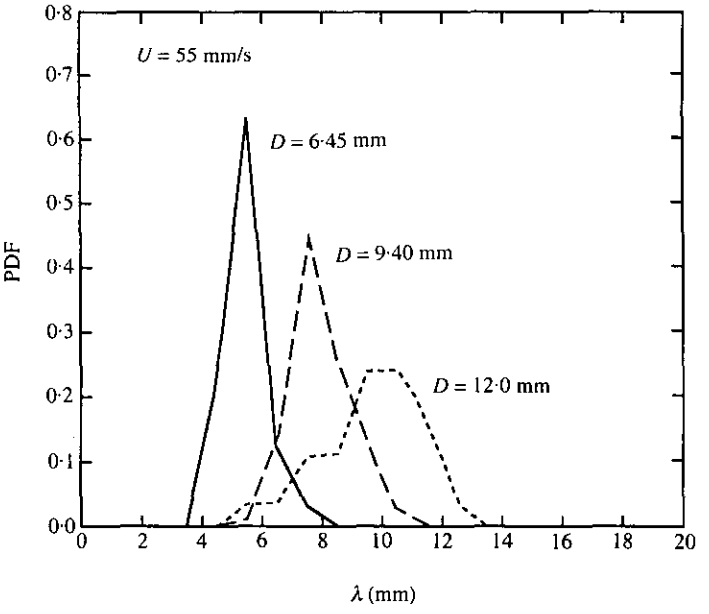

Figure 11. Probability density distribution of the spanwise wavelength: influence of the cylinder diameter.

The effect of applying spanwise perturbations upstream of the cylinder is shown in Figure 13. The freestream velocity was kept at $U = 0{\cdot}055$ m/s for all the perturbation experiments. Two types of perturbation were used: one was an array of delta-wings; the other was a screen made of fine wires. The spanwise perturbation wavelength and amplitudes were varied in the experiments.

With $D = 9{\cdot}4$ mm, the mean spanwise wavelength, λ, at the natural shedding was approximately 8 mm. It is shown that as the forcing wavelength was increased from 5 to 16 mm, λ did not follow the excitation wavelength, except near $\lambda \approx 8$ mm, where it shows a weak "locking" phenomenon. When perturbation levels of the delta-wing

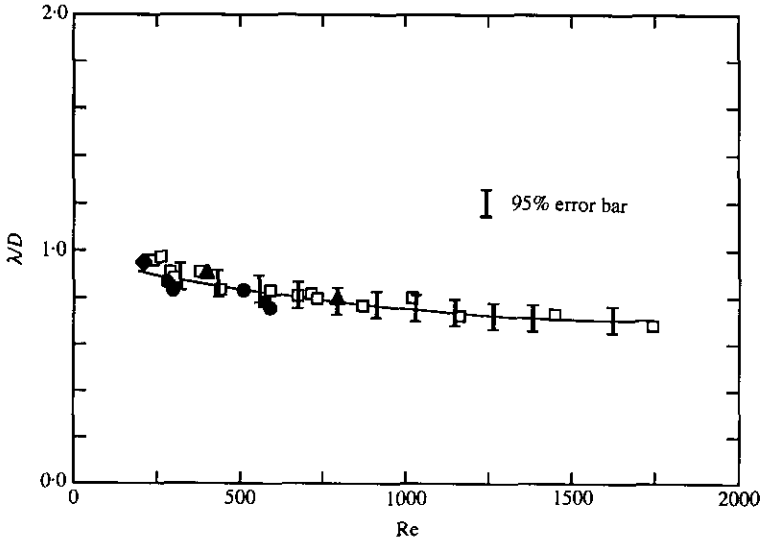

Figure 12. Mean spanwise wavelength variation with Reynolds number: natural shedding. ◆, $D = 3{\cdot}32$ mm; ●, $D = 6{\cdot}45$ mm; □, $D = 9{\cdot}40$ mm; ■, $D = 12{\cdot}0$ mm; ▲, $D = 12{\cdot}7$ mm.

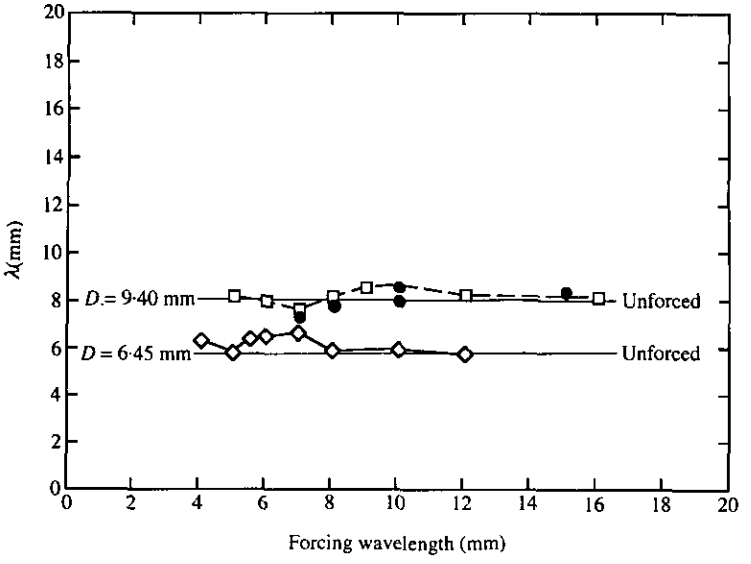

Figure 13. Spanwise wavelength, forced shedding. ◇, $D = 6{\cdot}45$ mm, delta-wing method; □, $D = 9{\cdot}40$ mm, delta-wing method; ●, $D = 9{\cdot}40$ mm, wire method; $U = 0{\cdot}055$ m/s.

array were raised from $\Delta h = 2{\cdot}0$ mm to $\Delta h = 5{\cdot}0$ mm (Figure 4), no influence on the spanwise wavelength could be observed. Similar trends were observed when a screen made of fine vertical wires (0·06 or 0·5 mm in diameter) at various spacings was placed upstream of the cylinder.

As the diameter of the cylinder was reduced to $D = 6{\cdot}4$ mm, the response curve shifted downward; the "locking region" also shifted to a smaller wavelength. This corresponds to a shift towards its "natural wavelength" of $\lambda \approx 5{\cdot}8$ mm. Therefore, the spacing of the structures changed when the diameter of the cylinder was varied, even at the excitation of the perturbations.

4. DISCUSSION

The evolution process of the streamwise vortices is postulated and conceptually shown in Figure 14, in a frame moving with the vortex street. According to this simplified

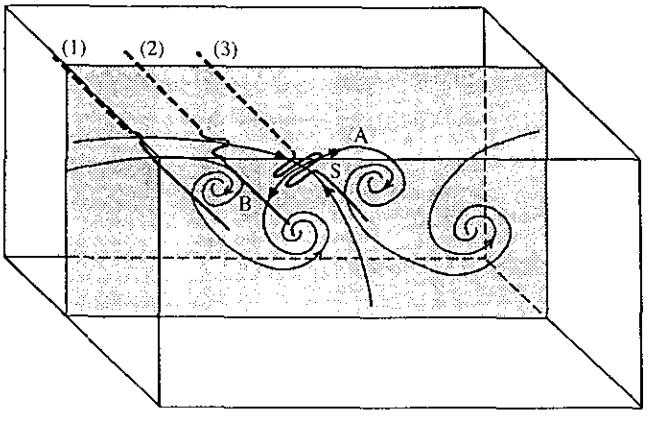

Figure 14. A conceptual interpretation of the amplification process of the streamwise vortices in a wake behind a bluff body: evolution of a vortex filament approaching the saddle region of the spanwise vortices. "S" denotes saddle point.

model, there are two fundamental elements: (1) a perturbed vorticity tube; and (2) a stretching region near the saddle point (denoted "S") formed by the primary rollers.

A fluid tube containing vorticity (vorticity tube) is located at position (1) initially, aligned with the spanwise direction. Due to nonuniformity of the flow, the vorticity tube is disturbed and develops a kink. As time elapses the perturbed vorticity moving at the local convection velocity arrives at position (2), and the amplitude of the "kink" grows due to self-induction of the tube, in accordance with the Biot–Savart law. As the distorted tube approaches the saddle point, the amplification of the vorticity intensifies due to the stretching effect of the spanwise vortices. This stretching is greatest when the vorticity tube is being "pulled apart" in the *opposite directions* along the diverging separatrix (Figure 14), since the flow in regions A and B is moving in opposite directions (in the moving frame). Although this hypothetical model is a simplification of the real process, and ignores the mutual interactions between the perturbed vorticity tubes and the effect of distortion of primary rollers (Strouhal vortex street), it shows conceptually the role of the Strouhal vortices in the development of the streamwise vortices, i.e. the vorticity amplification through stretching by the Strouhal vortices.

The above development process has also been demonstrated by Ashurst & Meiburg (1988) and Lasheras & Meiburg (1990), using three-dimensional vortex dynamics simulation method. The spanwise vorticity formed during the generation of the Strouhal vortex street can go through a process of reorientation and amplification to contribute to the development of the streamwise vorticity. This mechanism sets up a route through which mean kinetic energy of the flow is transferred into spinning motions of the streamwise vortices. Cantwell & Coles (1983) found that a substantial part of the turbulence production is concentrated near the saddles, primarily due to stretching of small-scale vorticity oriented along the diverging separatrices.

The orientations of the streamwise vortices measured from flow visualization images agree well with the above interpretation (see Figure 8). The locations of the streamwise vortices were confirmed to be in the braids joining two consecutive spanwise rollers. This is clearly shown in the photograph pair recorded simultaneously in the two orthogonal planes (Figure 6). The braids joining two consecutive Strouhal vortices are inclined structures containing streamwise vortices. This idea is supported by the results presented in Figure 8 which shows loci of the streamwise vortices. The orientations of the streamwise vortices are found to be inclined approximately $\pm 55°$ from the streamwise direction. This was obtained at a particular shedding phase at which image acquisition was triggered by a reference signal (from the hot-wire probe); some variation over the vortex-shedding cycle is expected. Nevertheless the data is in good agreement with hot-wire measurements of Zhou & Antonia (1992). It is therefore concluded that the streamwise vortices in the wake of the cylinder align in a zigzag manner wrapping around *opposite sign* spanwise rollers.

A further step towards the understanding of the dynamics of the streamwise vortices is to investigate their structural details. On important parameter characterizing the structure is the spanwise wavelength. From the results presented here it can be concluded that the spanwise wavelength of the structures scales with the cross-sectional size of the bluff body (e.g. cylinder diameter) and is weakly dependent on the Re (Figure 12). Contrary to Lasheras & Meiburg (1990) it was found that the spanwise wavelengths of the vortices are not broadband. The existence of a mean spanwise wavelength is clearly shown in the results of the spanwise perturbation study (Figure 13).

Vortex dynamics simulations (Ashurst & Meiburg 1988; Lasheras & Meiburg 1990) can interpret the amplification mechanism of the streamwise vorticity; however, they

are not capable of predicting the most-amplified spanwise wavelength of the streamwise vortex structures. To determine the spanwise wavelength at the initial stage of developing streamwise vortices requires three-dimensional linear instability calculations as used by Pierrehumbert & Widnall (1982) and more recently by Triantafyllou (1992).

Wei & Smith (1986), in their flow visualization investigation, found that the upstream streamwise vortices are locked onto the downstream streamwise vortices, leading them to speculate that some form of feedback mechanism is involved in the development of the streamwise vortices. It is possible a feedback of the disturbance from *developed* streamwise vortices at downstream locations could influence the *developing* streamwise vortices at upstream locations; such a process is consistent with the concept of an absolute instability mechanism (Monkewitz & Nguyen 1987). This is one possible explanation for the insensitivity of the spanwise spacing to the external perturbations.

5. CONCLUSION

The main feature of the three-dimensional near wake is the formation of counter-rotating streamwise vortical structures along the span of the cylinder. The mean spanwise wavelength of the vortical structures is found to scale with the diameter of the cylinder and is insensitive to forced spatial perturbations. The three-dimensional features of the streamwise vortices include vortex loops wrapping around the consecutive opposite-sign Strouhal vortices and their continual stretching motion along the diverging separatrix. Measurements from flow visualization and digital image studies have shown that the alignment of the streamwise vortices in the xy-plane is approximately $\pm 55°$ to the streamwise direction.

ACKNOWLEDGEMENTS

J. Wu and Dr J. Sheridan acknowledge the support from an Australia Research Council grant. J. Wu wishes to thank the CSIRO DBCE, Australia, for the use of their facilities. We wish to thank Mr N. Hamilton of CSIRO DBCE for producing the photographs presented in this paper.

REFERENCES

ASHURST, W. T. & MEIBURG, E. 1988 Three-dimensional shear layers via vortex dynamics. *Journal of Fluid Mechanics* **189,** 87–116.

BAYS-MUCHMORE, B. & AHMED. A. 1993 On streamwise vortices in turbulent wakes of cylinders. *Physics of Fluids* **A5,** 387–392.

BERNAL, L. P. & ROSHKO, A. 1986 Streamwise vortex structure in plane mixing layers, *Journal of Fluid Mechanics* **170,** 499–525.

CANTWELL, B. & COLES, D. 1983 An experimental study of entrainment and transport in the turbulent near wake of a circular cylinder. *Journal of Fluid Mechanics* **136,** 321–374.

COUTANCEAU, M. & R. DEFAYE, J. 1991 Circular cylinder wake configurations: a flow visualization survey. *Applied Mechanics Reviews* **44,** 255–305.

FERRE, J. A., MUMFORD, J. C., SAVILL, A. M. & CIRALT, F. 1990 Three-dimensional large-eddy motions and fine-scale activity in a plane wake. *Journal of Fluid Mechanics* **210,** 371–414.

GERRARD, J. H. 1978 The wakes of cylindrical bluff bodies at low Reynolds number. *Philosophical Transactions of the Royal Society of London* **288,** 351–382.

GRANT, M. L. 1958 The large eddies of turbulent motion. *Journal of Fluid Mechanics* **4,** 149–190.

HAMA, F. R. 1957 Three-dimensional vortex pattern behind a circular cylinder. *Journal of the Aeronautical Sciences,* 156–158.

HAMA, F. R. 1962 Streaklines in a perturbed shear flow. *Physics of Fluids* **5,** 644–650.

HUSSAIN, A. K. M. Fazle 1984 Coherent structures and incoherent turbulence. In *Turbulence and Chaotic Phenomena in Fluids* (ed. T. Tatsumi), pp. 453–460. Amsterdam: Elsevier.

LASHERAS, J. C. & MEIBURG, E. 1990 Three-dimensional vorticity modes in the wake of a flat plate. *Physics of Fluids* **A2,** 371–380.

LIN, S. J. & CORCOS, G. M. 1984 The mixing layer: deterministic models of a turbulent flow. Part 3. The effect of plane strain on the dynamics of streamwise vortices. *Journal of Fluid Mechanics* **141,** 139–178.

MONKEWITZ, P. A. & NGUYEN, L. N. 1987 Absolute instability in the near-wake of two-dimensional bluff bodies. *Journal of Fluids and Structures* **1,** 165–184.

NOACK, B. R. KÖNIG, M. & ECKELMANN, H. 1993 Three-dimensional stability analysis of the periodic flow around a circular cylinder. *Physics of Fluids* **A5,** 1279–1281.

NYGAARD, K. J. & GLEZER, A. 1991 Evolution of streamwise vortices and generation of small-scale motion in a plane mixing layer. *Journal of Fluid Mechanics* **231,** 257–301.

PIERREHUMBERT, R. T. & WIDNALL, S. E. 1982 The two- and three-dimensional instabilities of a spatially periodic shear layer. *Journal of Fluid Mechanics* **114,** 59–82.

TRIANTAFYLLOU, G. S. 1992 Three-dimensional flow patterns in two-dimensional wakes. *ASME Journal of Fluids Engineering* **114,** 356–361.

WEI, T. & SMITH, C. R. 1986 Secondary vortices in the wake of circular cylinders. *Journal of Fluid Mechanics* **169,** 513–533.

WELSH, M. C., SORIA, J., SHERIDAN, J., WU, J., HOURIGAN, K. & HAMILTON, N. 1992 Three-dimensional flows in the wake of a circular cylinder. *Album of Visualization,* No. 9, pp. 17–18. The Visualization Society of Japan.

WILLIAMSON, C. H. K. 1988 The existence of two stages in the transition to three-dimensionality of a cylinder wake. *Physics of Fluids* **31,** 3165–3168.

WILLIAMSON, C. H. K. 1989 Oblique and parallel modes of vortex shedding in the wake of a circular cylinder at low Reynolds number. *Journal of Fluid Mechanics* **206,** 579–627.

YOKOI, Y. & KAMEMOTO, K. 1992 Initial stage of three-dimensional vortex structure existing in a two-dimensional boundary layer separation flow. *JSME International Journal* **35**(2), 189–195.

ZHOU, Y. & ANTONIA, R. 1992 A study of flow properties near critical points. In *Eddy Structure Identification in Free Turbulent Shear Flows,* IUTAM Symposium, Poitiers, France, 14–16 October 1992, pp. IX.2.1–2.6.

APPENDIX: NOMENCLATURE

D	diameter of cylinder
Re	Reynolds number based on cylinder diameter and free-stream velocity
Re_{cr}	critical Reynolds number for the streamwise vortices to exist
t	time
T	period of the Strouhal vortex shedding
U	freestream velocity
x, y, z	streamwise, cross-flow and spanwise coordinates
λ	spanwise wavelength
Δh	size of the delta-wing